Published in final edited form as:
Biochemistry. 2009 May 26; 48(20): 4294–4304. doi:10.1021/bi900417b.

Modulation of molecular interactions and function by rhodopsin palmitylation†

Paul S.-H. Park[*,‡,§], **K. Tanuj Sapra**[▯,¶], **Beata Jastrzebska**[§], **Tadao Maeda**[‡,§], **Akiko Maeda**[§], **Wojciech Pulawski**[+], **Masahiro Kono**[#], **Janis Lem**[⊥], **Rosalie K. Crouch**[#], **Slawomir Filipek**[+,&], **Daniel J. Müller**[▯], and **Krzysztof Palczewski**[*,§]

[‡]Department of Ophthalmology and Visual Sciences, Case Western Reserve University, Cleveland, OH 44106 [§]Department of Pharmacology, Case Western Reserve University, Cleveland, OH 44106 [▯]Biotechnology Center, University of Technology, 01307 Dresden, Germany [⊥]Department of Ophthalmology, Program in Genetics, Program in Neuroscience, Molecular Cardiology Research Institute, Tufts Medical Center, Boston, MA 02111 [#]Department Ophthalmology, Medical University of South Carolina, Charleston, South Carolina 29425 [+]International Institute of Molecular and Cell Biology, 02-109 Warsaw, Poland [&]Faculty of Chemistry, University of Warsaw, 02-093, Warsaw, Poland

Abstract

Rhodopsin is palmitylated at two cysteine residues in its carboxyl terminal region. We have looked at the effects of palmitylation on the molecular interactions formed by rhodopsin using single-molecule force spectroscopy and the function of rhodopsin using both *in vitro* and *in vivo* approaches. A knockin mouse model expressing palmitate-deficient rhodopsin was used for live animal *in vivo* studies and to obtain native tissue samples for *in vitro* assays. We specifically looked at the effects palmitylation has on the chromophore-binding pocket, interactions of rhodopsin with transducin, and molecular interactions stabilizing the receptor structure. The structure of rhodopsin is largely unperturbed by the absence of palmitate linkage. The binding pocket for the chromophore 11-*cis*-retinal is minimally altered as palmitate-deficient rhodopsin exhibited the same absorbance spectrum as wild-type rhodopsin. Similarly, the rate of release of all-*trans*-retinal after light activation was the same both in the presence and absence of palmitylation. Significant differences were observed in the rate of transducin activation by rhodopsin and in the force required to unfold the last stable structural segment in rhodopsin at its carboxyl terminal region. A 1.3-fold reduction in the rate of transducin activation by rhodopsin was observed in the absence of palmitylation. Single-molecule force spectroscopy revealed a 2.1-fold reduction in normalized force required to unfold the carboxyl terminal end of rhodopsin. The absence of palmitylation in rhodopsin therefore destabilizes the

†This work was supported in part by U.S. Public Health Service grants EY018085, EY09339, GM079191, EY11373, EY004939, and EY12008 from the National Institutes of Health, Bethesda, MD. This work was also supported by the Deutsche Forschungsgemeinschaft (DFG), European Union, Polish Ministry of Science and Higher Education (grant no. N N301 2038 33), Ohio and Massachusetts Lions Eye Research Foundation, Foundation Fighting Blindness, an unrestricted grant from Amgen Inc., a Research to Prevent Blindness Challenge Grant to the Department of Ophthalmology at Tufts Medical Center, and unrestricted grants from Research to Prevent Blindness (New York) to the Department of Ophthalmology and Visual Sciences at Case Western Reserve University and the Department of Ophthalmology at Medical University of South Carolina. P. S.-H. P is the recipient of a Research to Prevent Blindness Career Development Award. R. K. C. is a Research to Prevent Blindness Senior Scientific Investigator.

*To whom correspondence should be addressed: Paul Shin-Hyun Park, Department of Ophthalmology and Visual Sciences, Case Western Reserve University, 2085 Adelbert Road, Pathology Room 312, Cleveland, OH 44106, Phone: 216-368-2533; Fax: 216-368-3171; E-mail: E-mail: paul.park@case.edu, Krzysztof Palczewski, Department of Pharmacology, Case Western Reserve University, 10900 Euclid Avenue, Cleveland, OH 44106, Phone: 216-368-4631; Fax: 216-368-1300; Email: E-mail: kxp65@case.edu.
¶Current address: Chemistry Research Laboratory, 12 Mansfield Road, OX1 3TA Oxford, UK

molecular interactions formed in the carboxyl terminal end of the receptor, which appears to hinder the activation of transducin by light-activated rhodopsin.

Many G protein-coupled receptors (GPCRs) are palmitylated at cysteine residues in the carboxyl terminal region. It is unclear what the precise role of palmitylation is both at the structural and functional levels. This fatty acid linkage has been implicated in various facets of GPCR function including coupling to and activation of the heterotrimeric G protein, receptor phosphorylation, internalization and desensitization, and localization of the receptor (1,2). Some receptors are dynamically palmitylated while others are constitutively palmitylated. There is no consensus among GPCRs on the role that palmitylation plays in receptor structure and function, which may reflect the different roles this covalent modification plays in different systems.

Rhodopsin is a prototypical member of the GPCR family (3,4). Much is known about this receptor both at the structural and functional levels. However, the role of palmitylation in the light receptor is still unclear. Rhodopsin is palmitylated at cysteine residues in the carboxyl terminal region at positions 322 and 323 in the bovine sequence. Several studies have been conducted in rhodopsin to understand the effect of palmitylation on its structure and function. The effects of palmitylation have been studied by either chemically removing the fatty acid linkage by treatment with either DTT or hydroxylamine or by mutating the cysteine residues that form the covalent fatty acid linkage and expressing the mutant receptor in a heterologous expression system (5–9). Apparent palmitylation-related changes have been observed under certain conditions in some of these studies. For instance, the absence of palmitylation has been shown to affect transducin activation, rhodopsin regeneration, and cause small changes to structure and stability. Some of these effects, however, are not consistently observed among different studies, which points to the difficulties in teasing out effects due to chemical treatment or expression in a heterologous system with those that are truly endogenous to the fatty acid linkage itself.

To circumvent secondary effects on receptor structure and function, a knockin mouse model was generated expressing palmitate-deficient rhodopsin that was mutated in cysteine residues at positions 322 and 323 (10). Initial characterization of these mice suggested that rhodopsin becomes hyperphosphorylated upon light activation and that the shut-off of the system is enhanced. We have utilized this model system to further probe the effects palmitylation has on the structure and function of rhodopsin. This knockin mouse has allowed us to study palmitate-deficient rhodopsin collected from native retinal tissue. We have looked at the structural impact of palmitylation using single-molecule force spectroscopy (SMFS) to specifically monitor changes to molecular interactions formed within the receptor. At the functional level, we have looked at the effects palmitylation has on the chromophore and the binding-pocket environment of rhodopsin, interactions of light-activated rhodopsin with transducin, and rod photoreceptor physiology.

EXPERIMENTAL PROCEDURES

Isolation of disc membranes from rod outer segments (ROS)

All experimental procedures were conducted under dim red light. All centrifugation steps were performed at 4 °C. ROS were purified from the retina of wild-type C57BL/6 mice or knockin mice expressing palmitate-deficient rhodopsin as described previously (11). Generation of knockin mice expressing palmitate-deficient rhodopsin was described previously (10). Mice were 6–8 weeks old and 12–15 mice were used for each preparation of purified ROS. Mice were dark adapted by maintaining them in darkness overnight.

Disc membranes were collected by osmotically bursting purified ROS. Purified ROS were resuspended in 1 mL buffer A (2 mM Tris-HCl, pH 7.4) and incubated overnight at 4 °C. The membrane suspension was centrifuged at 16,100 × *g* for 5 min and the supernatant discarded. The membrane pellet was washed twice with 1 mL buffer A and three times with buffer B (2 mM Tris-HCl, 150 mM NaCl, 2 mM EDTA, pH 7.4). Each time the membrane pellet was resuspended by homogenizing with a hand-held pestle and centrifuged at 16,100 × *g* for 5 min. The washed disc membranes were resuspended in buffer A and examined by SMFS or were resuspended in buffer C (67 mM potassium phosphate, 1 mM magnesium acetate, 0.1 mM EDTA, 18 % sucrose, pH 7.0) and stored at − 80 °C. Membranes stored at − 80 °C were thawed and washed twice in buffer A prior to use. Concentration of rhodopsin in the disc membrane was determined by solubilizing an aliquot of isolated membranes in 20 mM Bis-Tris propane, 40 mM CHAPS (Anatrace, Inc., Maumee, OH), pH 7.5, and reading the absorbance at 500 nm on a Hewlett-Packard 8452A UV-visible spectrophotometer. A molar extinction coefficient of 40,600 $M^{-1}\cdot cm^{-1}$ (12) was used to compute rhodopsin concentration.

Purification of rhodopsin from mouse eyes

Eyes from 3 dark-adapted mice (6–8 weeks old) were used for each purification. Eyes were homogenized in 3 mL buffer D (10 mM Bis-Tris propane, 150 mM NaCl, pH 7.5) using a hand-held glass homogenizer. The homogenate was centrifuged at 125,000 × *g* for 5 min. The pellet was resuspended in buffer E (10 mM Bis-Tris propane, 500 mM NaCl, 20 mM *n*-dodecyl-β-D-maltoside (Anatrace, Inc., Maumee, OH), pH 7.5) and shaken at room temperature for 15 min. The suspension was then centrifuged at 125,000 × *g* for 20 min. The supernatant was loaded on a 4.5 × 29 mm column of anti-1D4 antibody coupled to CNBr-activated Sepharose 4B preequilibrated with buffer F (10 mM Bis-Tris propane, 500 mM NaCl, 2 mM *n*-dodecyl-β-D-maltoside, pH 7.5). Anti-1D4 antibody recognizes the carboxyl terminus of bovine rhodopsin (13). The column was washed with 10 mL of buffer F. Purified rhodopsin was obtained by eluting the column with buffer F supplemented with 800 μM of 1D4 peptide (TETSQVAPA) synthesized by United Biochemical Research, Inc. (Seattle, WA). The absorbance spectrum of purified rhodopsin was obtained using a Hewlett-Packard 8452A UV-visible spectrophotometer. The concentration of rhodopsin was calculated by measuring the absorbance at 500 nm and using a molar extinction coefficient of 40,600 $M^{-1}\cdot cm^{-1}$ (12).

Single-molecule force spectroscopy

SMFS was performed on ROS disc membranes isolated from mice as described previously for bovine samples (14,15). Disc membranes were adsorbed on freshly cleaved mica and SMFS was conducted using NPS Si_3N_4 cantilevers (nominal spring constant 0.06 N/m; Veeco Metrology, Santa Barbara, CA). Spring constants of the cantilevers were determined in buffer solution using a Picoforce atomic force microscope (Veeco Metrology). Force-distance curves were obtained using a Multimode atomic force microscope (Veeco Metrology). All SMFS experiments were performed at room temperature (≈21 °C) in SMFS assay buffer (150 mM KCl, 25 mM $MgCl_2$, 20 mM Tris, pH 7.8). Force-distance curves were analyzed using criteria established previously (15). Force peaks were analyzed using the worm-like chain model assuming a persistence length of 0.4 nm (16). The number of amino acid residues stretched above the membrane surface was estimated from the contour length obtained from worm-like chain model fits and assuming an amino acid residue length of 0.36 nm.

Metarhodopsin II (MII) decay assay

Assays were conducted using 10 nM of purified rhodopsin in 20 mM Bis-Tris propane, 120 mM NaCl, 2 mM *n*-dodecyl-β-D-maltoside, pH 6.0. Rhodopsin was bleached for 15 s using a Fiber-Lite illuminator and a 480–520 nm band pass filter. Intrinsic tryptophan fluorescence was then immediately monitored on a Perkin-Elmer LS55 fluorescence spectrometer using an

excitation wavelength of 295 nm (2.5 nm slit) and an emission wavelength of 330 nm (5 nm slit). The temperature of the cuvette was maintained at 20 °C with a circulating water bath. The increase in tryptophan fluorescence is correlated with the release of all-*trans*-retinal from the binding pocket in rhodopsin (17). Fluorescence data was analyzed on Sigma-Plot (Systat Software, Inc., San Jose, CA) by non-linear regression fitting to an equation describing first order reaction kinetics to obtain the time constant τ. Statistical significance between data was assessed by a two-tailed student's t-Test.

Transducin activation assay – native disc membranes

Transducin was purified from fresh bovine ROS as described previously (18). Transducin concentration was determined by Bradford assay (Bio-Rad, Hercules, CA). Purified transducin and rhodopsin in disc membranes were mixed at a concentration of 250 nM and 30 nM, respectively, in buffer G (20 mM Bis-Tris propane, 120 mM NaCl, 6 mM $MgCl_2$, pH 6.0). Samples were bleached for 15 s with a Fiber-Lite illuminator and a 480–520 nm band pass filter and then incubated for 400 s with continuous low-speed stirring. The cuvette containing the sample was maintained at 20 °C using a circulating water bath throughout the assay. Activation of transducin was initiated by the addition of GTPγS at a final concentration of 5 μM. Intrinsic tryptophan fluorescence was monitored on a Perkin-Elmer LS55 fluorescence spectrometer using an excitation wavelength of 300 nm (5 nm slit) and an emission wavelength of 345 nm (8 nm slit). Increased tryptophan fluorescence has been shown to correlate with the guanyl nucleotide exchange that occurs in transducin upon its activation (19,20). Fluorescence data were analyzed on Sigma-Plot (Systat Software, Inc., San Jose, CA) by non-linear regression fitting to an equation describing first order reaction kinetics to obtain the rate constant *k*. Statistical significance between data was assessed by a two-tailed student's t-Test.

Transducin activation assay – COS cell membranes

Wild-type and Cys322Ser/Cys323Ser bovine rod opsin were transiently expressed in COS cells (21). Membranes from transfected COS cells were isolated as described previously (22,23). The amount of opsin in the membrane preparations was determined by slot blot analysis using known amounts of bovine rhodopsin as a reference and probed with the anti-1D4 antibody (23).

The ability of rhodopsin and opsin to activate transducin was determined using a radioactive filter-binding assay under pseudo first order conditions (22,23). The reaction mixture (50 μL final volume) contained 4 nM opsin, 2.5 μM transducin, 3.0 μM [^{35}S]GTPγS, 20 μM 11-*cis*-retinal, 10 mM 2-(N-morpholino)ethanesulfonic acid (pH 6.4), 100 mM NaCl, 1 mM DTT, and 5 mM $MgCl_2$, pH 6.4. All components of the reaction mixture except 11-*cis*-retinal and [^{35}S]GTPγS were first mixed. 11-*cis*-retinal was added from a stock dissolved in ethanol 1 min prior to addition of [^{35}S]GTPγS. Light-independent transducin activation rates were first determined over a 5 min period after the addition of [^{35}S]GTPγS. Light-dependent transducin activation rates were then determined over a 30 s period immediately after illuminating the reaction mixture for 6 s with light (> 495 nm).

Electroretinography (ERG) and retinoid analysis

Single-flash ERG recordings on mice under scotopic and photopic conditions and recovery of dark adaptation assays were performed as described previously (24). Extraction, derivatization, and separation on HPLC of retinoids from mouse eyes were performed as described previously (24).

Molecular dynamics simulations

Minimizations and molecular dynamics simulations were performed using the program CHARMM (25). A united-atom forcefield (CHARMM19 (26)) was used with an implicit membrane/water model IMM1 (27). The latter is an extension of the EEF1 implicit water model to heterogeneous membrane/aqueous media (28). In the IMM1 method the water/membrane system is achieved by changing solvation reference parameters along the line perpendicular to the membrane. There is an area 0.6 nm in thickness between water and membrane environments that allows for gradual changes in properties between them. At the hydrophobic border of this layer, 90% of the environment derives from the hydrophobic core. At the water border, 90% of the environment derives from bulk water properties. Since these properties change according to a sigmoidal function, there is no sharp change of properties. The implicit solvent method reduces the number of degrees of freedom that are necessary for the evaluation of energy and force, which allows for more efficient sampling of phase space than explicit solvent methods. Differences in the movement of Helix 8 in palmitylated and unpalmitylated rhodopsin are small. These small changes may be undetectable in rugged systems such as those that include explicit phospholipid molecules. The IMM1 method with immobile membrane area allows for the investigation of small differences both in internal parameters and in relation to the membrane border.

The structure of rhodopsin used in simulations was downloaded from Protein Data Bank (Protein Data Bank ID: 1U19) (29). The initial placement of monomeric rhodopsin in the membrane interior and the membrane thickness (3.2 nm) were based on Orientations of Proteins in Membranes (OPM) database (30). However, during minimization and initial stages of molecular dynamics (up to 5 ns) rhodopsin was moved perpendicular to the membrane by about 0.4 nm. Thus, productive molecular dynamics simulations started from newly formed equilibrium. To assess the influence of palmitates and to assure statistical validity, 32 independent 30 ns simulations were performed: 16 simulations were conducted for palmitylated rhodopsin and 16 simulations were conducted for unpalmitylated rhodopsin. The temperature was set to 300 K and was controlled with Langevine thermostat (friction coefficient was set to 5 ps^{-1}). The bonds involving hydrogen atoms were constrained using the SHAKE algorithm, allowing an integration time step of 2 fs. The systems were heated to 300 K with 3 K rise every 5000 steps during 500,000 steps. After heating, the systems were allowed to equilibrate for 1 ns. We adopted the parameterization of retinal and palmitates described previously (31–35), and we adjusted these parameters for IMM1. The solvation parameters for retinal and palmityl chains were set up according to similar atom types in IMM1.

RESULTS

Effect of palmitylation on the chromophore of rhodopsin

Rhodopsin contains two palmitate groups that are linked to cysteine residues at positions 322 and 323. Knockin mice were generated previously that introduced point mutations resulting in the replacement of the wild-type cysteine residues to serine (position 322) or threonine (position 323) (10). The mutation of cysteine residues resulted in rhodopsin molecules that lacked palmitate linkages. These knockin mice therefore provide an excellent model to study the effects of the palmitate linkage on the structure and function of rhodopsin in native tissue and without the need for chemical modification.

Knockin mice expressing palmitate-deficient rhodopsin generate rod outer segments with rhodopsin properly targeted to this location. Rhodopsin was purified from whole eye extracts obtained from wild-type and knockin mice. The pigment was purified on an affinity column packed with anti-1D4 antibody conjugated to Sepharose. The antibody specifically detects the last 8 amino acid residues of bovine and mouse rhodopsin. The mobility of wild-type and

palmitate-deficient rhodopsin on SDS-PAGE were similar (Figure 1A). The absorbance spectrum for both types of rhodopsin exhibited a peak at about 500 nm (Figure 1B). The lack of palmitylation therefore does not affect the environment surrounding the conjugated chromophore.

Activation of rhodopsin by light results in the formation of the active MII state. The decay of rhodopsin from the MII state can be monitored by measuring the increase in tryptophan fluorescence that occurs when all-*trans*-retinal exits the binding pocket (17). The decay of the MII state was measured for purified rhodopsin (Figures 1C and 1D). The rate of MII decay was similar for both wild-type and palmitate-deficient rhodopsin. Thus, the exit of chromophore from the binding pocket after activation is unaffected by the absence of the palmitate groups.

The complement of retinoids in the eye after exposing mice to light was determined by HPLC analysis. Rhodpsin is conjugated by a Schiff base linkage in transmembrane Helix 7 to the chromophore 11-*cis*-retinal, which acts as an inverse agonist locking the receptor in the inactive state (36). Upon capture of a photon of light, 11-*cis*-retinal is photoisomerized to all-*trans*-retinal. This photoconversion initiates the activation of the receptor molecule. All-*trans*-retinal is subsequently released from the binding pocket of the receptor and enters into the retinoid cycle that leads to the regeneration of 11-*cis*-retinal (37). Once released from rhodopsin, all-*trans*-retinal is cleared from the disc membrane and into the cytoplasm where it is enzymatically reduced. The conversion of 11-*cis*-retinal to all-*trans*-retinal and the clearance of all-*trans*-retinal were monitored in mice (Figure 2). Dark-adapted mice were exposed to lighting conditions that bleached about 70% of rhodopsin in the eye. Retinoids were extracted from the eyes of dark-adapted mice at different time points after illumination and were analyzed by HPLC to monitor the time course of retinoid flow. The lack of palmitylation does not affect the amount of 11-*cis*-retinal converted to all-*trans*-retinal nor does it affect the clearance of all-*trans*-retinal. Thus, the initial events of receptor activation is unaffected by the lack of palmitate linkage.

Effect of palmitylation on the interaction with tranducin

Rhodopsin contains an amphiphilic helix at its carboxyl terminal region that lies peripherally to the membrane. Helix 8 is important for the coupling and activation of the G protein transducin. The palmitate linkage is commonly thought to act as an anchor holding Helix 8 in place. We determined the ability of rhodopsin to activate transducin indirectly under *in vivo* conditions and directly under *in vitro* conditions.

The visual function of mice was tested by ERG. The ERG response to different intensities of light was measured both under scotopic and photopic conditions (Figure 3). We quantified the amplitude of the resulting a-wave and b-wave, which are indicative of the electrical signal originating from the photoreceptor and secondary retinal neurons, including bipolar cells, respectively. There was no significant difference in ERG response between mice expressing wild-type rhodopsin with those expressing palmitate-deficient rhodopsin at the intensities of light tested. Thus, the lack of palmitylation in rhodopsin does not significantly affect its ability to produce the physiological response in the retina upon light activation. The normal ERG responses indicate that rhodopsin is able to couple to and activate transducin thereby initiating the phototransduction cascade.

The ability of mice to dark adapt after exposure to intense illumination was monitored by measuring the recovery in the amplitude of the a-wave resulting from single-flash ERG (Figure 4). Mice were illuminated with intense light that resulted in the bleaching of about 70% of rhodopsin in the eye. The mice were then placed in the dark and single-flash ERG responses were recorded every 5 minutes. The recovery of the a-wave amplitude was measured to

determine the time course of dark adaptation. The ability of mice expressing palmitate-deficient rhodopsin was significantly attenuated compared to wild-type mice. While palmitylation does not affect significantly the ability of rhodopsin to activate and produce a maximal physiological response, it does affect the ability of the photoreceptors to dark-adapt and be primed for signaling again.

We looked directly at the interaction between rhodopsin and transducin under *in vitro* conditions. Retinas from mice were collected and rod outer segments purified. Disc membranes were released from the outer segments by osmotic bursting and washed. Rhodopsin in disc membranes was examined for its ability to activate transducin. A fluorescence-based approach was used to monitor the guanyl nucleotide exchange in the alpha subunit in transducin that occurs upon its activation by rhodopsin. A small but significant difference was observed between the rates of transducin activation promoted by wild-type and palmitate-deficient rhodopsin. Palmitate-deficient rhodopsin was 1.34 times slower in activating transducin compared to wild-type rhodopsin (Figure 5). Transducin activation rates were also determined by a radioactive filter binding assay using bovine opsin heterologously expressed in COS cells. Palmitate-deficient opsin was expressed in COS cells by mutating cysteine residues at position 322 and 323 to serine residues. Minimal transducin activation was detected in the dark with COS cell membranes containing opsin or rhodopsin (opsin reconstituted with 11-*cis*-retinal) for both wild-type and unpalmitylated forms (Figure 6). Light activation of rhodopsin resulted in transducin activation rates for the wild-type receptor that was 1.71 times faster than the unpalmitylated mutant. Thus, measurements made with both native and COS cell membranes indicate that the absence of palmitylation diminishes the ability of rhodopsin to activate transducin.

Changes in molecular interactions caused by the absence of palmitylation in rhodopsin

SMFS allows direct probing and structural assignment of molecular interactions that have been established in membrane proteins under near-native conditions (38). Rhodopsin in the discs of bovine rod outer segments has been investigated previously by SMFS to reveal the molecular interactions that stabilize the light receptor (15). SMFS has revealed that the structure of rhodopsin is organized into distinct structural segments that exhibit intrinsic stability to unfolding. The force required to unfold these regions indicates the strength of the interactions that stabilize structural segments of the receptor. However, the composition of inter- and intra-molecular interactions that contribute to the stability of individual structural segments remains unknown. We previously noted in initial characterizations of bovine rhodopsin that the stable structural segment formed by the carboxy terminal end might be co-stabilized by the anchoring of palmitates attached to cysteine residues at position 322 and 323. Here, we tested this hypothesis by characterizing disc membranes obtained from mice expressing palmitate-deficient rhodopsin. SMFS was carried out on disc membrane samples obtained from the retina of wild-type and palmitate-deficient rhodopsin mice. Force-distance curves were recorded and analyzed using procedures previously established for bovine rhodopsin and other membrane proteins (15).

Analyses of wild-type and palmitate-deficient rhodopsin from mice revealed force peaks in force-distance curves that assigned stable structural segments of the receptor. We focused our analysis on force peaks corresponding to structural segments previously assigned in bovine rhodopsin (15). The location of those structural segments in the secondary structure of rhodopsin is shown in Figure 7A. Both wild-type and palmitate-deficient rhodopsin revealed these structural segments. The average force and detection frequency of each force peak that denoted a structural segment was determined for both types of rhodopsin (Figures 8A and 8B). The force required to unfold each structural segment is indicative of the stability in that region of the receptor.

Similar to bovine rhodopsin, the most stable structural segment in both wild-type and palmitate-deficient mouse rhodopsin was segment H3,H4,C2,E2 (Figures 8A and 8B). This structural segment was detected in every force-distance curve analyzed and required an average force of 157 pN and 169 pN to unfold in wild-type and palmitate-deficient rhodopsin, respectively. The difference in average unfolding force between the two types of rhodopsin studied for each structural segment analyzed is summarized in Figure 8C. All segments except for segment CT showed small differences ranging from 16 pN to 12 pN. Segment CT exhibited the largest difference in average unfolding force. Palmitate-deficient rhodopsin required 36 pN less force to unfold in this segment compared to wild-type rhodopsin. In contrast to differences in average unfolding force, more structural segments exhibited large differences in detection frequency between the two types of rhodopsin (Figure 8D). Once again, segment CT exhibited the largest difference in detection frequency with the detection of molecular interactions stabilizing this region being less frequent in palmitate-deficient rhodopsin by 21%. Segments N1 and H6.2 also had large differences in detection frequency between the two types of rhodopsin. Molecular interactions in N1 and H6.2 were detected 14% and 18% less frequently, respectively, in force curves for palmitate-deficient rhodopsin compared to wild-type rhodopsin.

The two structural segments in the immediate vicinity of the palmitylated cysteine residues are H8 and CT. The average force required to unfold segment H8 in wild-type and palmitate-deficient rhodopsin is 91 pN and 89 pN, respectively, and the frequency of detection in both types of rhodopsin was 56% and 60%, respectively. Thus, there was very little change in either average unfolding force or detection frequency between wild-type and palmitate-deficient rhodopsin, which indicates that the molecular interactions formed in this region are the same in both types of rhodopsin and that the palmitate linkage is unnecessary for the formation and stability of this helix. Both mouse rhodopsin forms exhibited a force peak corresponding to segment CT, which was previously thought to derive its stability, at least in part, by the anchoring into the membrane by covalently linked palmitate groups (15). This segment exhibited the largest difference between wild-type and palmitate-deficient rhodopsin in both average unfolding force (36 pN) and frequency of detection (21%) (Figures 8C and 8D). The average force required to unfold this structural segment was 113 pN and 77 pN for wild-type and palmitate-deficient rhodopsin, respectively. Thus, the absence of palmitylation causes segment CT to become less stable and significantly changes the molecular interactions that stabilize this region.

The average unfolding force was multiplied by the detection frequency for each structural segment to compute the normalized force (39). The normalized force factors in both average unfolding force and detection frequency and therefore differences in normalized force will represent a more complete picture of the changes occurring in molecular interactions under different conditions. The difference in normalized force for each analyzed structural segment between the two types of rhodopsin was calculated (Figure 8E). The largest difference occurred in segment CT with palmitate-deficient rhodopsin exhibiting a decrease in normalized force by 41 pN. All other analyzed structural segments displayed smaller differences in normalized force indicating that the stability of rhodopsin is largely unchanged in the absence of palmitylation except for the region making up segment CT (Figure 7B).

DISCUSSION

Rhodopsin is naturally palmitylated on cysteine residues at positions 322 and 323 at its carboxyl terminal end. We have used a knockin mouse model expressing palmitate-deficient rhodopsin to investigate the effect of the palmitate groups on the structure and function of the light receptor. This mouse model has allowed us to obtain samples from native retinal tissue and avoid effects associated with chemical processing of samples. For instance, we have observed

that treatment of disc membranes with 1M hydroxylamine (e.g., (9)) disrupts the membrane structure resulting in an inability to detect disc structures by AFM (data not shown). Thus, while hydroxylamine treatment may not affect the receptor molecule itself, it does have the potential to alter other properties such as membrane structure. These changes to the membrane may have led to the differences observed in the literature for the effects attributed to the palmitylation of rhodopsin such as differences measured in the level of regeneration of rhodopsin by 11-*cis*-retinal between rhodopsin mutated at Cys322 and Cys323 versus hydroxylamine-treated rhodopsin (8,9). In the current investigation, we characterized both the functional and structural effects palmitylation has on rhodopsin.

Chromophore-binding pocket of rhodopsin unchanged in the absence of palmitylation

The different regions in the structure of rhodopsin do not exist or function independently of each other and therefore changes in molecular interactions in one region of the protein can potentially have effects on the molecular interactions in other regions (40). This interdependency has been demonstrated in mutations in rhodopsin that cause instability and misfolding of the protein, which leads to *retinitis pigmentosa*, and in the stabilizing effects of zinc ions on the structure of the light receptor (14,41,42), where changes in one region of the protein affect other areas of the protein far removed. Thus, we looked at whether a change occurring in the carboxyl terminal region of the protein would affect properties in the binding pocket of 11-*cis*-retinal, which is situated within the transmembrane helices closer to the extracellular surface of the receptor.

Characterization of palmitate-deficient rhodopsin obtained from knockin mice indicates that the absence of the fatty acid linkage does not significantly affect the properties or environment surrounding bound 11-*cis*-retinal. Purified rhodopsin from wild-type and palmitate-deficient rhodopsin mice exhibit identical absorbance spectra and rates of release of the chromophore upon light activation (Figure 1). The levels of retinal as assessed by HPLC of extracts from eyes of mice are also similar (Figure 2). At the level of structure, minimal changes in molecular interactions were observed in structural segments involved in the chromophore-binding pocket (Figure 7B). Thus, the lack of palmitate linkage does not affect the ability of rhodopsin to bind 11-*cis*-retinal or to release all-*trans*-retinal from the binding pocket after receptor activation.

This lack of effect related to the chromophore is consistent with studies of palmitate-deficient rhodopsin heterologously expressed in COS-1 cells, where palmitates were removed by mutating cysteine residues at positions 322 and 323 to serine residues. The absence of palmitate groups did not affect the ability of the mutant rhodopsin to bind chromophore or change the absorbance spectra and extinction coefficient (8). It is also consistent with observations made with other GPCRs that bind small molecule ligands within the transmembrane helices in a similar location as 11-*cis*-retinal in rhodopsin (43–48). The absence of palmitylation in these GPCRs did not significantly affect the affinity for ligands, even in cases where the absence of palmitylation affected activation of the G protein (43–46). Thus, palmitylation does not appear to significantly affect the environment surrounding the chromophore in rhodopsin or ligand-binding pocket in other GPCRs.

Effect of palmitylation on the structure of rhodopsin is mainly localized to the carboxyl terminal region

SMFS analysis revealed that molecular interactions stabilizing structural segments that are distal from the palmitate groups are largely unaffected (Figure 7B and Figure 8). Thus, palmitylation does not appear to significantly affect the molecular interactions of rhodopsin as a whole. This is consistent with previous circular dichroism studies on rhodopsin that showed that the absence of palmitylation does not cause any gross structural changes in rhodopsin (6). Segments H8 and CT are the two structural segments that are in the direct vicinity of the

cysteine residues covalently linked to palmitate groups (Figure 7A). Since the effect of palmitylation appears to be localized to the immediate region where the fatty acid linkage occurs, the molecular interactions stabilizing these two regions would be the ones most likely affected. Segment H8 is upstream of the palmitate linkage and is entirely composed of Helix 8, which is an amphiphilic helix at the carboxyl terminal region of rhodopsin that lies peripherally to the membrane. Segment CT occurs immediately after the cysteine residues that are palmitylated.

Helix 8 can adopt its helical structure independently from the receptor but requires the presence of the lipid bilayer (49–52). Palmitylation in rhodopsin and other GPCRs is often thought to anchor the carboxyl terminal region to the lipid bilayer and allow Helix 8 to maintain interaction with the surface of the membrane (2). Segment H8 exhibited minimal difference between wild-type and palmitate-deficient rhodopsin in average unfolding force, detection frequency, and normalized force (Figure 7B and Figure 8). The absence of change in this structural segment suggests that the molecular interactions stabilizing this region, including those present within the helical structure and those involved in interactions with the membrane, do not require palmitylation. Thus, in contrast to previous assumptions, the adoption of a helical structure and the maintenance of interaction with the membrane by Helix 8 appear to be independent of palmitylation.

The ability of Helix 8 to adopt its proper structure and maintain contact with the lipid bilayer in the absence of palmitylation is consistent with the fact that not all GPCRs are palmitylated such as the middle/long wavelength cone opsin, which is still predicted to form Helix 8 (53). It is also consistent with a spin-labeling study investigating the mobility of the carboxyl terminal region of rhodopsin, which indicated that palmitylation is not the sole determinant in anchoring this region of the protein to the lipid bilayer (54). Molecular dynamics simulations were conducted to test further these notions that contrast previously held views (Figure 9). Within the limitations of the simulation times, significant changes were absent in the position of transmembrane helices and in the structure of Helix 8 in the absence of palmitylation. In addition, Helix 8 maintained contact with the membrane throughout the simulations. Helix 8, however, was more mobile without palmitate anchorage and sampled a wider range of positions during the simulation period, which may contribute to the differences in transducin activation rate discussed later.

We had previously attributed the detection of molecular interactions assigned to segment CT to the anchoring of the protein into the membrane by the palmitate groups in this region (15). If the origin of stability is solely due to the anchoring of this structural region of the receptor to the membrane, then the absence of palmitylation in rhodopsin in our preparations should not exhibit a peak in force-distance curves corresponding to this region. Segment CT was detected in SMFS data from palmitate-deficient rhodopsin, which suggests that palmitylation is not the only determinant in stabilizing this region. In contrast to segment H8, segment CT exhibited the largest difference among structural segments in average unfolding force, detection frequency, and normalized force between the two types of rhodopsin tested (Figure 7B and Figure 8). The average unfolding force and detection frequency were greatly reduced compared to wild-type rhodopsin, indicating the absence of palmitylation significantly alters the molecular interactions formed in this region, which results in destabilization. Thus, while palmitylation is not the sole determinant of stabilizing segment CT, its absence significantly destabilizes this region of the receptor.

Functional consequences of the destabilization of carboxyl terminal region

The absence of palmitylation and destabilization of segment CT appears to have several functional consequences in rhodopsin. Both wild-type and palmitate-deficient rhodopsin can promote transducin activation under both *in vivo* and *in vitro* conditions (Figure 3, Figure 5,

and Figure 6). Palmitate-deficient rhodopsin is 1.3–1.7-fold slower in activating transducin compared to wild-type rhodopsin in *in vitro* assays. Exposed regions on the cytoplasmic surface of rhodopsin can interact with transducin and affect its activity. Helix 8 plays an important role in the interaction of rhodopsin with and activation of transducin (7). Molecular interactions stabilizing segment H8, which encompasses Helix 8, are largely unchanged in the absence of palmitylation and therefore likely do not contribute to the difference observed in transducin activation. Likewise, large changes are absent in structural segments that include the exposed cytoplasmic loops in rhodopsin, thereby suggesting that these regions also do not significantly contribute to the differences observed in *in vitro* transducin activation assays. Since the largest effect on the structure of rhodopsin occurs in segment CT, the less efficient transducin activity promoted by palmitate-deficient rhodopsin is likely a result of the destabilization that occurs in the carboxyl terminal region.

The effects observed in previous studies of rhodopsin palmitylation on the activity of transducin are different from those observed in the current study. Rod outer segment membranes treated with DTT to remove palmitate groups do not show significant changes in transducin activation rates (5). In contrast to guanyl nucleotide exchange rates, the rate of light-induced GTPase activity of transducin was increased in palmitate-deficient rhodopsin from rod outer segment membranes treated with hydroxylamine (9). This effect appears to be dependent on the nature of the preparation or presence of the membrane since light-induced GTPase activity of transducin was unaffected by the absence of palmitylation in purified preparations of depalmitylated receptor (8). Purification and depalmitylation procedures can disrupt the native organization of rhododpsin and thereby prevent the detection of changes we have observed in native rod outer segment and COS cell membranes.

Although a small difference is observed in *in vitro* transducin activation assays, a significant change is not detectable in the physiological response of the rod photoreceptors in ERG recordings (Figure 3). Likewise, suction electrode recordings of single rod photoreceptor cells from the same knockin mice do not show significant differences in the rising phase and time to peak of the response (10). Thus, the diminished transducin activation observed *in vitro* in the absence of palmitylation is not large enough to significantly affect the physiological response of the rod photoreceptor cells.

The absence of palmitylation in rhodopsin affects the recovery of photoreceptors after light stimulation. Monitoring the recovery of the a-wave after exposing mice to intense light that bleaches about 70 % of rhodopsin showed that dark adaptation is delayed in mice expressing palmitate-deficient rhodopsin (Figure 4). This delayed recovery after strong bleaching in ERG recordings is consistent with single-cell suction recordings of rod photoreceptors that showed the recovery of the response to be incomplete at higher intensity flashes in the absence of palmitylation in rhodopsin (10). The rate of clearance of all-*trans*-retinal from rhodopsin and the disc membranes is unchanged in mice expressing wild-type or palmitate-deficient rhodopsin (Figure 2). The delayed dark adaptation in rod photoreceptors of mice expressing palmitate-deficient rhodopsin is therefore likely due to properties related to the rhodopsin molecule itself. Since the largest change in rhodopsin structure caused by the absence of palmitylation occurs as a destabilization of the carboxyl terminal region, the delayed dark adaptation after strong bleaching conditions may be related to the destabilization of this region.

In contrast to strong lighting conditions, dim flashes of light results in a faster recovery of the response in single-cell recordings of photoreceptors expressing palmitate-deficient rhodopsin (10). This enhanced shut-off has been thought to be related to the increased level of receptor phosphorylation observed upon light stimulation in palmitate-deficient rhodopsin mice. Palmitylation and the level of phosphorylation appear to be correlated in GPCRs (1). The mechanism leading to this increased phosphorylation is unclear. The residues in rhodopsin

phosphorylated by rhodopsin kinase are present in segment CT. The destabilization in segment CT in the absence of palmitylation may release steric hindrance of rhodopsin kinase interactions thereby allowing rhodopsin to become hyperphosphorylated.

Concluding remarks

The availability of knockin mice expressing palmitate-deficient rhodopsin has made it possible to conduct detailed structural and functional studies on the effect palmitylation has on rhodopsin activity and rod photoreceptor physiology. The absence of palmitylation does not significantly affect the molecular interactions within rhodopsin as a whole, but rather, is localized to molecular interactions at the carboxyl terminal end. The destabilization in the carboxyl terminal region observed in the absence of palmitylation appears to affect the interactions with transducin and play a role in altered dark adaptation. The inefficient transducin activation caused by the absence of palmitylation does not result in any detectable difference in the physiological response of rod photoreceptor cells and the effects on dark adaptation observed in the absence of rhodopsin palmitylation likely will not be critical for humans under normal conditions. While the absence of palmitylation in rhodopsin alone may not critically affect human vision under normal conditions, it may have more drastic consequences under prolonged extreme lighting conditions or under conditions where there are alterations or mutations in other molecules or proteins involved in phototransduction or the retinoid cycle.

Abbreviations

AFM, atomic force microscope/microscopy; ERG, electroretinography; GPCR, G protein-coupled receptor; MII, metarhodopsin II; ROS, rod outer segment; SMFS, single-molecule force spectroscopy.

ACKNOWLEDGMENT

We would like to thank Alejandro T. Colozo for help with preparation of some figures.

REFERENCES

1. Qanbar R, Bouvier M. Role of palmitoylation/depalmitoylation reactions in G-protein-coupled receptor function. Pharmacol Ther 2003;97:1–33. [PubMed: 12493533]
2. Torrecilla I, Tobin AB. Co-ordinated covalent modification of G-protein coupled receptors. Curr Pharm Des 2006;12:1797–1808. [PubMed: 16712489]
3. Ridge KD, Palczewski K. Visual rhodopsin sees the light: structure and mechanism of g protein signaling. J Biol Chem 2007;282:9297–9301. [PubMed: 17289671]
4. Palczewski K. G protein-coupled receptor rhodopsin. Annu Rev Biochem 2006;75:743–767. [PubMed: 16756510]
5. Sachs K, Maretzki D, Meyer CK, Hofmann KP. Diffusible ligand all-trans-retinal activates opsin via a palmitoylation-dependent mechanism. J Biol Chem 2000;275:6189–6194. [PubMed: 10692411]
6. Traxler KW, Dewey TG. Effects of depalmitoylation on physicochemical properties of rhodopsin. Biochemistry 1994;33:1718–1723. [PubMed: 8110774]
7. Marin EP, Krishna AG, Zvyaga TA, Isele J, Siebert F, Sakmar TP. The amino terminus of the fourth cytoplasmic loop of rhodopsin modulates rhodopsin-transducin interaction. J Biol Chem 2000;275:1930–1936. [PubMed: 10636894]
8. Karnik SS, Ridge KD, Bhattacharya S, Khorana HG. Palmitoylation of bovine opsin and its cysteine mutants in COS cells. Proc Natl Acad Sci U S A 1993;90:40–44. [PubMed: 8419942]
9. Morrison DF, O'Brien PJ, Pepperberg DR. Depalmitylation with hydroxylamine alters the functional properties of rhodopsin. J Biol Chem 1991;266:20118–20123. [PubMed: 1939072]

10. Wang Z, Wen XH, Ablonczy Z, Crouch RK, Makino CL, Lem J. Enhanced shutoff of phototransduction in transgenic mice expressing palmitoylation-deficient rhodopsin. J Biol Chem 2005;280:24293–24300. [PubMed: 15851469]
11. Nickell S, Park PS, Baumeister W, Palczewski K. Three-dimensional architecture of murine rod outer segments determined by cryoelectron tomography. J Cell Biol 2007;177:917–925. [PubMed: 17535966]
12. Wald G, Brown PK. The molar extinction of rhodopsin. J Gen Physiol 1953;37:189–200. [PubMed: 13109155]
13. Molday RS, MacKenzie D. Monoclonal antibodies to rhodopsin: characterization, cross-reactivity, and application as structural probes. Biochemistry 1983;22:653–660. [PubMed: 6188482]
14. Park PS, Sapra KT, Kolinski M, Filipek S, Palczewski K, Muller DJ. Stabilizing effect of Zn2+ in native bovine rhodopsin. J Biol Chem 2007;282:11377–11385. [PubMed: 17303564]
15. Sapra KT, Park PS, Filipek S, Engel A, Muller DJ, Palczewski K. Detecting molecular interactions that stabilize native bovine rhodopsin. J Mol Biol 2006;358:255–269. [PubMed: 16519899]
16. Rief M, Gautel M, Oesterhelt F, Fernandez JM, Gaub HE. Reversible unfolding of individual titin immunoglobulin domains by AFM. Science 1997;276:1109–1112. [PubMed: 9148804]
17. Farrens DL, Khorana HG. Structure and function in rhodopsin. Measurement of the rate of metarhodopsin II decay by fluorescence spectroscopy. J Biol Chem 1995;270:5073–5076. [PubMed: 7890614]
18. Jastrzebska B, Maeda T, Zhu L, Fotiadis D, Filipek S, Engel A, Stenkamp RE, Palczewski K. Functional characterization of rhodopsin monomers and dimers in detergents. J Biol Chem 2004;279:54663–54675. [PubMed: 15489507]
19. Phillips WJ, Cerione RA. The intrinsic fluorescence of the alpha subunit of transducin. Measurement of receptor-dependent guanine nucleotide exchange. J Biol Chem 1988;263:15498–15505. [PubMed: 3049609]
20. Fahmy K, Sakmar TP. Regulation of the rhodopsin-transducin interaction by a highly conserved carboxylic acid group. Biochemistry 1993;32:7229–7236. [PubMed: 8343512]
21. Oprian DD. Expression of opsin genes in COS cells. Methods in Neurosciences 1993;15:301–306.
22. Robinson PR. Assays for detection of constitutively active opsins. Methods Enzymol 2000;315:207–218. [PubMed: 10736704]
23. Kono M. Constitutive activity of a UV cone opsin. FEBS Lett 2006;580:229–232. [PubMed: 16368093]
24. Maeda A, Maeda T, Imanishi Y, Kuksa V, Alekseev A, Bronson JD, Zhang H, Zhu L, Sun W, Saperstein DA, Rieke F, Baehr W, Palczewski K. Role of photoreceptor-specific retinol dehydrogenase in the retinoid cycle in vivo. J Biol Chem 2005;280:18822–18832. [PubMed: 15755727]
25. Brooks, Bernard R.; R E B; Olafson, Barry D.; States, David J.; Swaminathan, S.; Karplus, Martin. CHARMM: A program for macromolecular energy, minimization, and dynamics calculations. J Comput Chem 1983;4:187–217.
26. Neria E, Fischer S, Karplus M. Simulation of activation free energies in molecular systems. The Journal of Chemical Physics 1996;105:1902–1921.
27. Lazaridis T. Effective energy function for proteins in lipid membranes. Proteins 2003;52:176–192. [PubMed: 12833542]
28. Lazaridis T, Karplus M. Effective energy function for proteins in solution. Proteins 1999;35:133–152. [PubMed: 10223287]
29. Okada T, Sugihara M, Bondar AN, Elstner M, Entel P, Buss V. The retinal conformation and its environment in rhodopsin in light of a new 2.2 A crystal structure. J MolBiol 2004;342:571–583.
30. Lomize MA, Lomize AL, Pogozheva ID, Mosberg HI. OPM: orientations of proteins in membranes database. Bioinformatics 2006;22:623–625. [PubMed: 16397007]
31. Tajkhorshid E, Suhai S. Influence of the Methyl Groups on the Structure, Charge Distribution, and Proton Affinity of the Retinal Schiff Base. The Journal of Physical Chemistry B 1999;103:5581–5590.

32. Tajkhorshid E, Baudry J, Schulten K, Suhai S. Molecular dynamics study of the nature and origin of retinal's twisted structure in bacteriorhodopsin. Biophys J 2000;78:683–693. [PubMed: 10653781]
33. Nina M, Roux B, Smith JC. Functional interactions in bacteriorhodopsin: a theoretical analysis of retinal hydrogen bonding with water. Biophys J 1995;68:25–39. [PubMed: 7711248]
34. Baudry J, Crouzy S, Roux B, Smith JC. Quantum Chemical and Free Energy Simulation Analysis of Retinal Conformational Energetics. Journal of Chemical Information and Computer Sciences 1997;37:1018–1024.
35. Tajkhorshid E, Paizs B, Suhai S. Conformational Effects on the Proton Affinity of the Schiff Base in Bacteriorhodopsin: A Density Functional Study. The Journal of Physical Chemistry B 1997;101:8021–8028.
36. Park PS, Lodowski DT, Palczewski K. Activation of G protein-coupled receptors: beyond two-state models and tertiary conformational changes. Annu Rev Pharmacol Toxicol 2008;48:107–141. [PubMed: 17848137]
37. Travis GH, Golczak M, Moise AR, Palczewski K. Diseases caused by defects in the visual cycle: retinoids as potential therapeutic agents. Annu Rev Pharmacol Toxicol 2007;47:469–512. [PubMed: 16968212]
38. Kedrov A, Janovjak H, Sapra KT, Muller DJ. Deciphering molecular interactions of native membrane proteins by single-molecule force spectroscopy. Annu Rev Biophys Biomol Struct 2007;36:233–260. [PubMed: 17311527]
39. Cisneros DA, Oberbarnscheidt L, Pannier A, Klare JP, Helenius J, Engelhard M, Oesterhelt F, Muller DJ. Transducer binding establishes localized interactions to tune sensory rhodopsin II. Structure 2008;16:1206–1213. [PubMed: 18682222]
40. Klein-Seetharaman J. Dual role of interactions between membranous and soluble portions of helical membrane receptors for folding and signaling. Trends Pharmacol Sci 2005;26:183–189. [PubMed: 15808342]
41. Hwa J, Garriga P, Liu X, Khorana HG. Structure and function in rhodopsin: packing of the helices in the transmembrane domain and folding to a tertiary structure in the intradiscal domain are coupled. Proc Natl Acad Sci U S A 1997;94:10571–10576. [PubMed: 9380676]
42. Hwa J, Klein-Seetharaman J, Khorana HG. Structure and function in rhodopsin: Mass spectrometric identification of the abnormal intradiscal disulfide bond in misfolded retinitis pigmentosa mutants. Proc Natl Acad Sci U S A 2001;98:4872–4876. [PubMed: 11320236]
43. Hayashi MK, Haga T. Palmitoylation of muscarinic acetylcholine receptor m2 subtypes: reduction in their ability to activate G proteins by mutation of a putative palmitoylation site, cysteine 457, in the carboxyl-terminal tail. Arch.Biochem.Biophys 1997;340:376–382. [PubMed: 9143344]
44. O'Dowd BF, Hnatowich M, Caron MG, Lefkowitz RJ, Bouvier M. Palmitoylation of the human beta 2-adrenergic receptor. Mutation of Cys341 in the carboxyl tail leads to an uncoupled nonpalmitoylated form of the receptor. J Biol Chem 1989;264:7564–7569. [PubMed: 2540197]
45. Renner U, Glebov K, Lang T, Papusheva E, Balakrishnan S, Keller B, Richter DW, Jahn R, Ponimaskin E. Localization of the mouse 5-hydroxytryptamine(1A) receptor in lipid microdomains depends on its palmitoylation and is involved in receptor-mediated signaling. Mol Pharmacol 2007;72:502–513. [PubMed: 17540717]
46. Papoucheva E, Dumuis A, Sebben M, Richter DW, Ponimaskin EG. The 5-hydroxytryptamine(1A) receptor is stably palmitoylated, and acylation is critical for communication of receptor with Gi protein. J Biol Chem 2004;279:3280–3291. [PubMed: 14604995]
47. Jin H, Zastawny R, George SR, O'Dowd BF. Elimination of palmitoylation sites in the human dopamine D1 receptor does not affect receptor-G protein interaction. Eur.J.Pharmacol 1997;324:109–116. [PubMed: 9137920]
48. Kennedy ME, Limbird LE. Mutations of the alpha 2A-adrenergic receptor that eliminate detectable palmitoylation do not perturb receptor-G-protein coupling. J Biol Chem 1993;268:8003–8011. [PubMed: 8385131]
49. Yeagle PL, Alderfer JL, Albert AD. Structure determination of the fourth cytoplasmic loop and carboxyl terminal domain of bovine rhodopsin. Mol Vis 1996;2:12. [PubMed: 9238089]

50. Choi G, Guo J, Makriyannis A. The conformation of the cytoplasmic helix 8 of the CB1 cannabinoid receptor using NMR and circular dichroism. Biochim Biophys Acta 2005;1668:1–9. [PubMed: 15670725]

51. Choi G, Landin J, Xie XQ. The cytoplasmic helix of cannabinoid receptor CB2, a conformational study by circular dichroism and (1)H NMR spectroscopy in aqueous and membrane-like environments. J Pept Res 2002;60:169–177. [PubMed: 12213126]

52. Katragadda M, Maciejewski MW, Yeagle PL. Structural studies of the putative helix 8 in the human beta(2) adrenergic receptor: an NMR study. Biochim Biophys Acta 2004;1663:74–81. [PubMed: 15157609]

53. Stenkamp RE, Filipek S, Driessen CA, Teller DC, Palczewski K. Crystal structure of rhodopsin: a template for cone visual pigments and other G protein-coupled receptors. Biochim Biophys Acta 2002;1565:168–182. [PubMed: 12409193]

54. Langen R, Cai K, Altenbach C, Khorana HG, Hubbell WL. Structural features of the C-terminal domain of bovine rhodopsin: a site-directed spin-labeling study. Biochemistry 1999;38:7918–7924. [PubMed: 10387033]

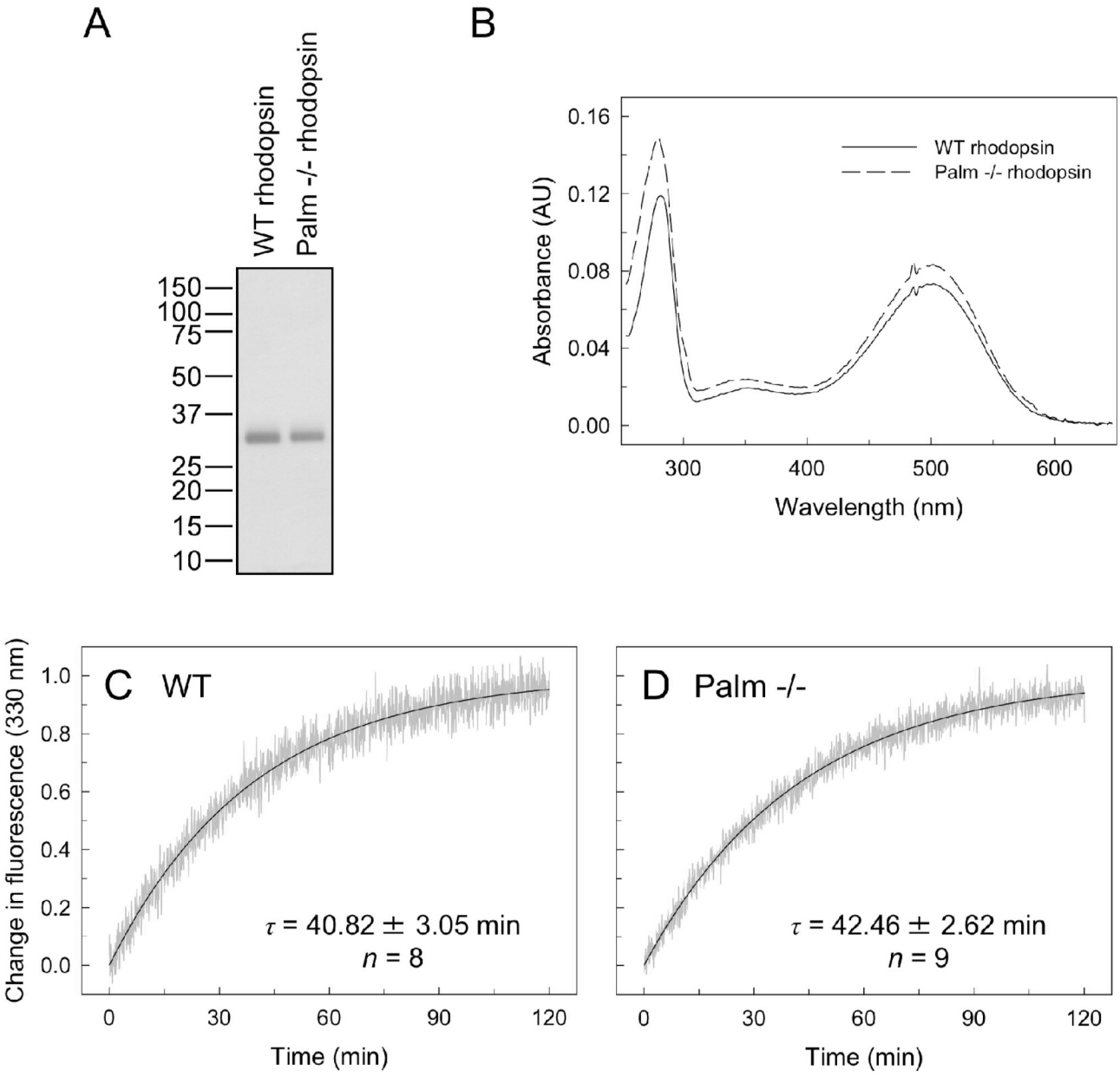

FIGURE 1.

Characterization of purified rhodopsin. Rhodopsin was purified from whole eye extracts of wild-type (WT) and palmitate-deficient rhodopsin knockin (palm −/−) mice by affinity purification on an anti-1D4 antibody column. (A) Purified rhodopsin was run on an SDS-PAGE gel and detected by silver staining. (B) The absorbance spectra of rhodopsin from wild-type mice and palmitate-deficient mice. Both spectra show the characteristic maximal peak for rhodopsin at about 500 nm. (C) and (D) The change in tryptophan fluorescence was monitored after light activation of rhodopsin to measure the rate of chromophore release from the binding pocket. The data (gray) were fit by non-linear regression (black curve) to obtain the time constant τ. The average τ values are shown with the standard deviations for the number of

experiments indicated (*n*). The difference in the time constant was not statistically significant ($p = 0.25$) between wild-type and palmitate-deficient rhodopsin.

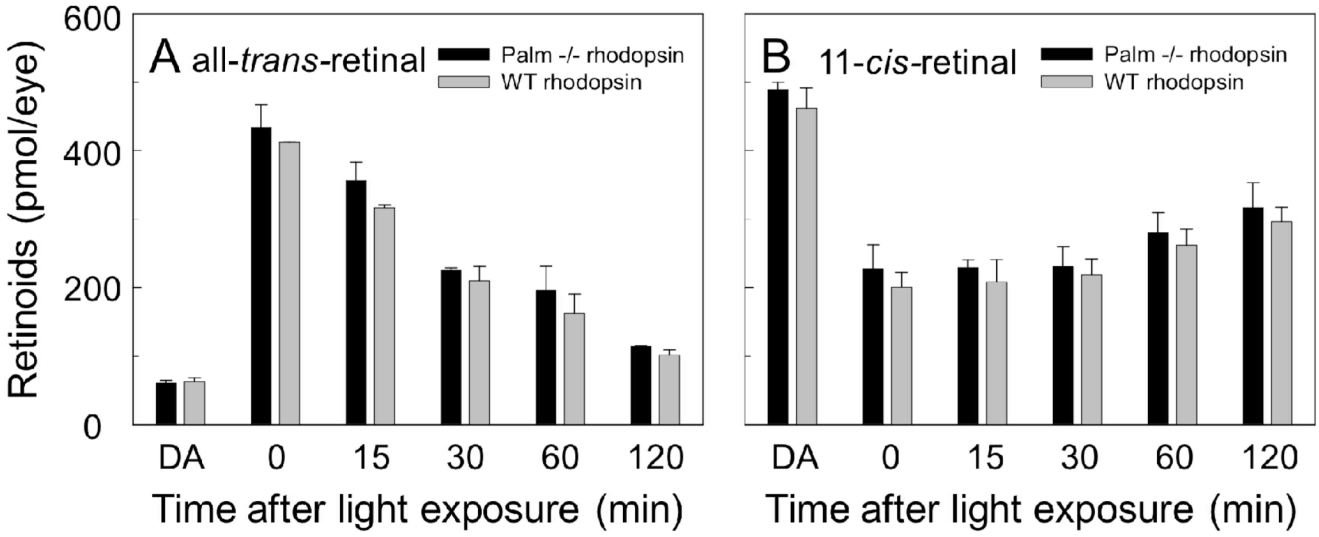

FIGURE 2.

Retinoid analysis. Dark-adapted (DA) mice were illuminated with light to bleach about 70% of rhodopsin molecules. Retinoids were extracted from eyes after the times from light exposure indicated and quantified by HPLC. Shown are the average levels (± SD) of all-*trans*-retinal (A) and 11-*cis*-retinal (B) in the eyes of mice collected at different time periods after light exposure. Extracts from three mice were used to calculate the average level of retinoids at each time point except the 30 min time point where six mice were used. Both male and female mice were used and were 6 weeks old.

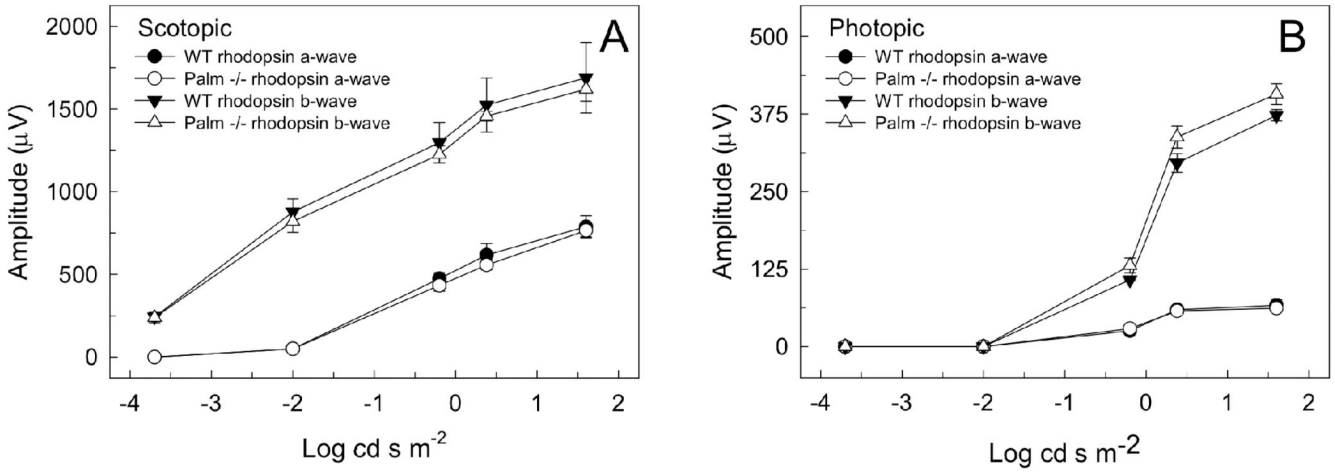

FIGURE 3.

ERG responses. ERG responses were recorded from mice expressing wild-type and palmitate-deficient rhodopsin under scotopic (A) and photopic (B) conditions. Each point represents the average response from each eye of three mice (± SEM). Male mice were used that were 6 weeks of age.

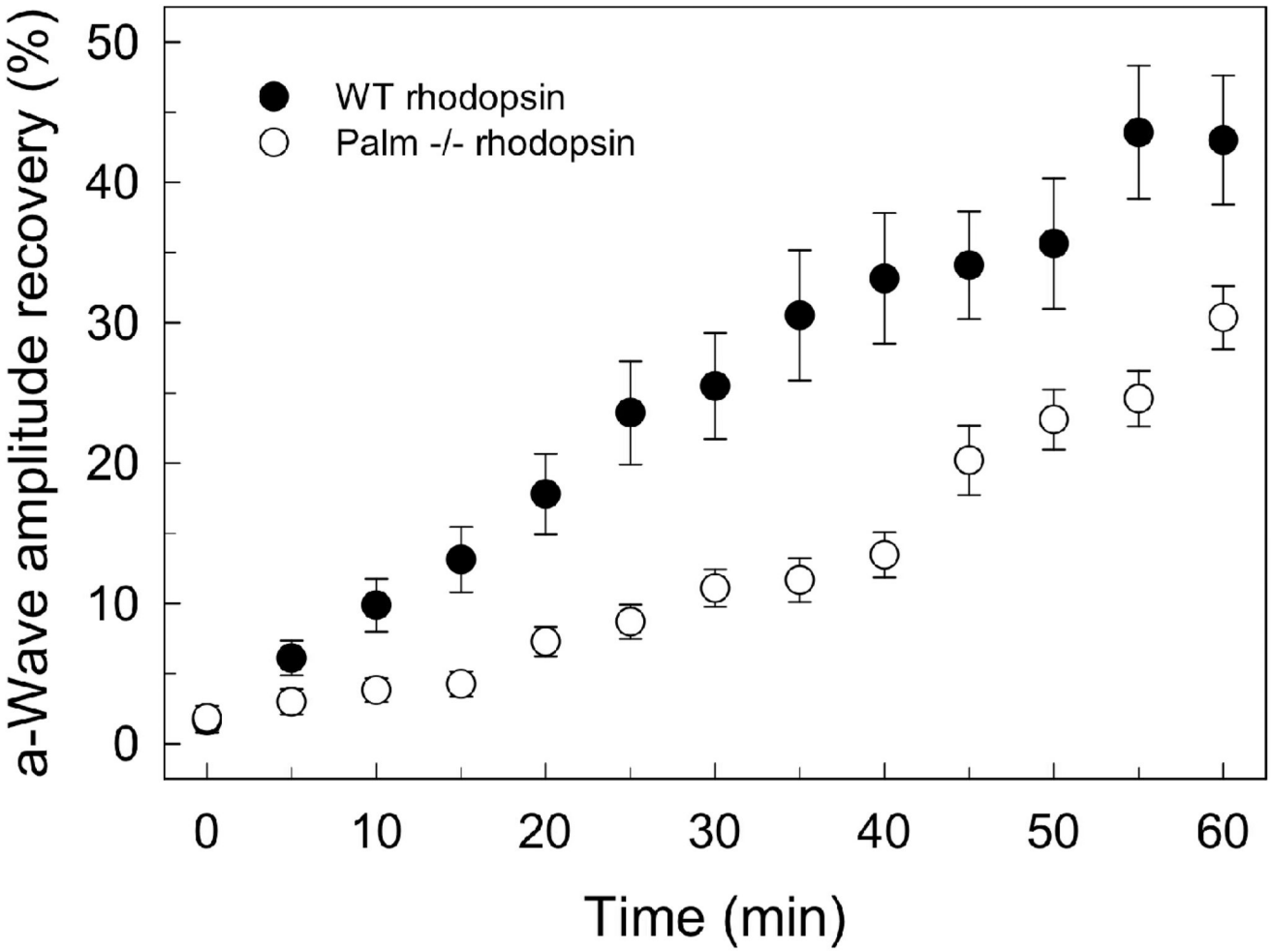

FIGURE 4.

Dark adaptation after intense bleaching. Dark-adapted mice were bleached for 3 min with intense light (500 cd·m^{-2}), which bleaches approximately 70% of rhodopsin. Recovery of the a-wave amplitude was monitored with single-flash ERG at an illumination intensity of −0.2 log cd·s·m^{-2}. Each time point represents the average a-wave recovery (± SD) measured in 6 (WT) or 7 (Palm −/−) male mice 6 weeks of age.

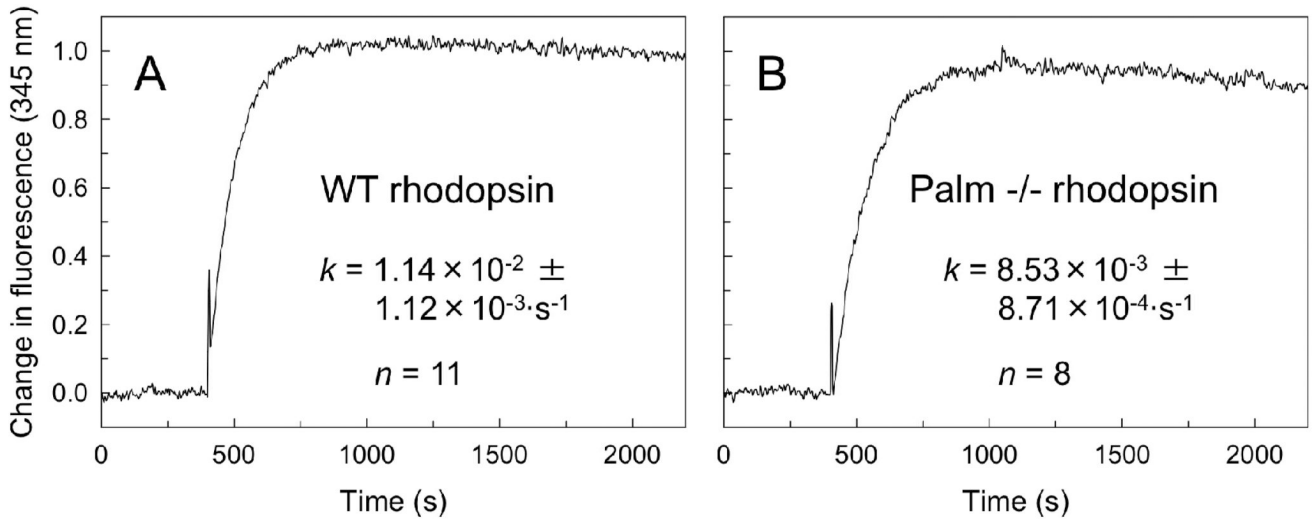

FIGURE 5.

Transducin activation by mouse rhodopsin in ROS disc membranes. ROS disc membranes were prepared from mice expressing wild-type (A) and palmitate-deficient (B) rhodopsin as outlined in the Materials and Methods section. The exchange of guanyl nucleotides in transducin was monitored by tryptophan fluorescence. GTPγS was added 400 s after light-activation of rhodopsin. The data were fit by non-linear regression to an exponential rise model to obtain the rate constant, *k*. The average values are shown with the standard deviation for the number of experiments indicated. The number of different preparations of membranes used to compute the average values in A and B was 4 and 3, respectively. The difference observed in transducin activation rates between wild-type and palmitate-deficient rhodopsin was statistically significant ($p \leq 0.0001$).

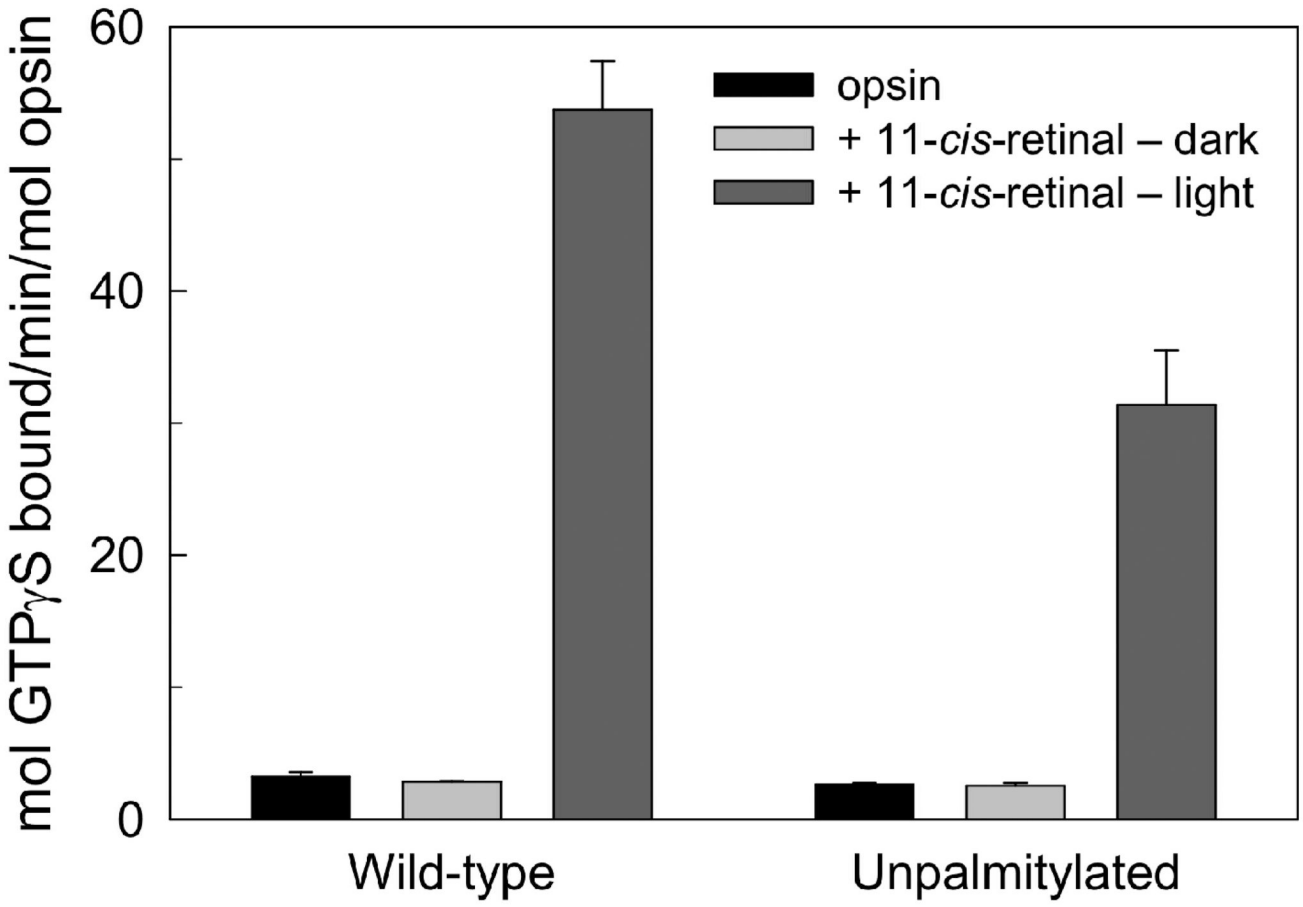

FIGURE 6.

Transducin activation by bovine rhodopsin in COS cell membranes. Wild-type and unpalmitylated (Cys322Ser/Cys323Ser) bovine opsin were expressed in COS cells. The rate of incorporation of [^{35}S]GTPγS was monitored in a suspension containing COS cell membranes and transducin by a radioactive filter binding assay. Rates were determined for opsin, dark-adapted rhodopsin (+ 11-*cis*-retinal – dark), and light-activated rhodopsin (+ 11-*cis*-retinal – light). The average (± SEM) rates from data collected in triplicate are shown (*n* = 3). Activity was not corrected for basal transducin activation at this pH.

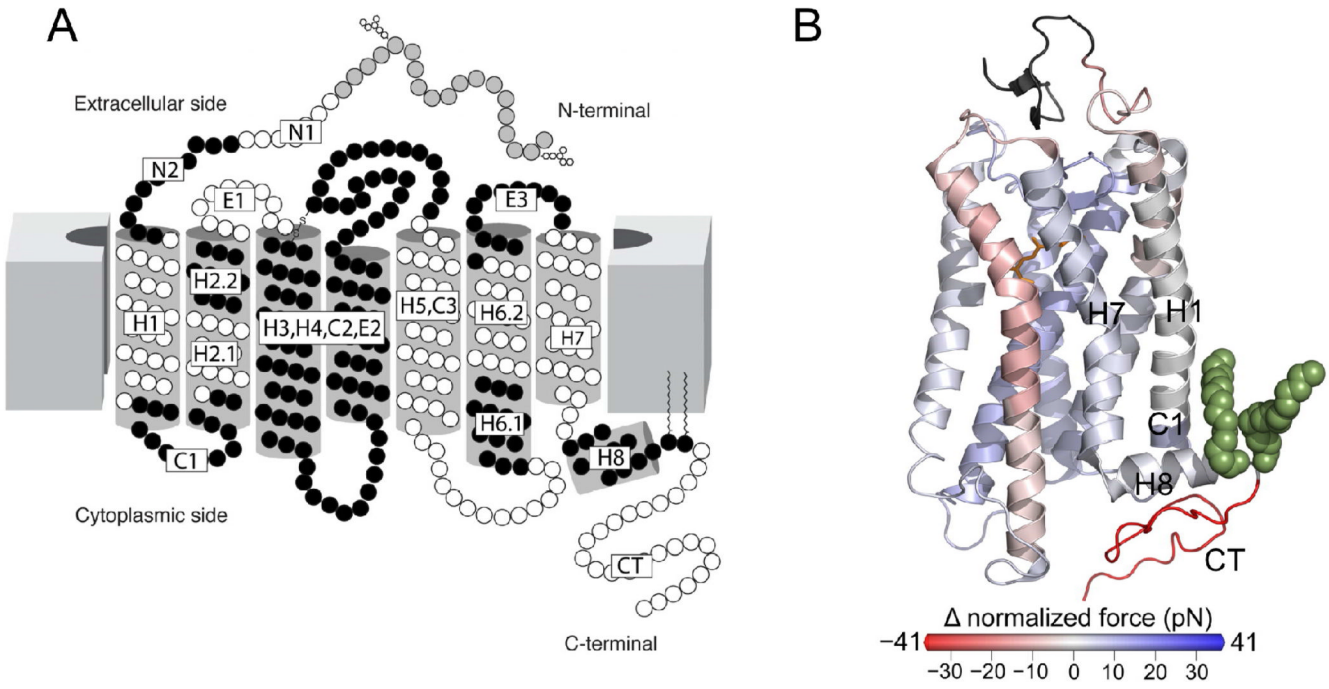

FIGURE 7.

Stable structural segments of rhodopsin. (A) Stable structural segments assigned previously for bovine rhodopsin (15) are shown on the secondary structure of rhodopsin. The segments are colored in white and black with the identifying segment name indicated. (B) The difference in normalized force between palmitate-deficient and wild-type rhodopsin for each stable structural segment is highlighted on the structure of bovine rhodopsin (Protein Data Bank ID: 1U19). Segments with a lower or greater normalized force in palmitate-deficient rhodopsin are shown in red and blue, respectively. Palmitate groups are colored in green and 11-*cis*-retinal is colored in orange. Segments near the palmitate groups are labeled.

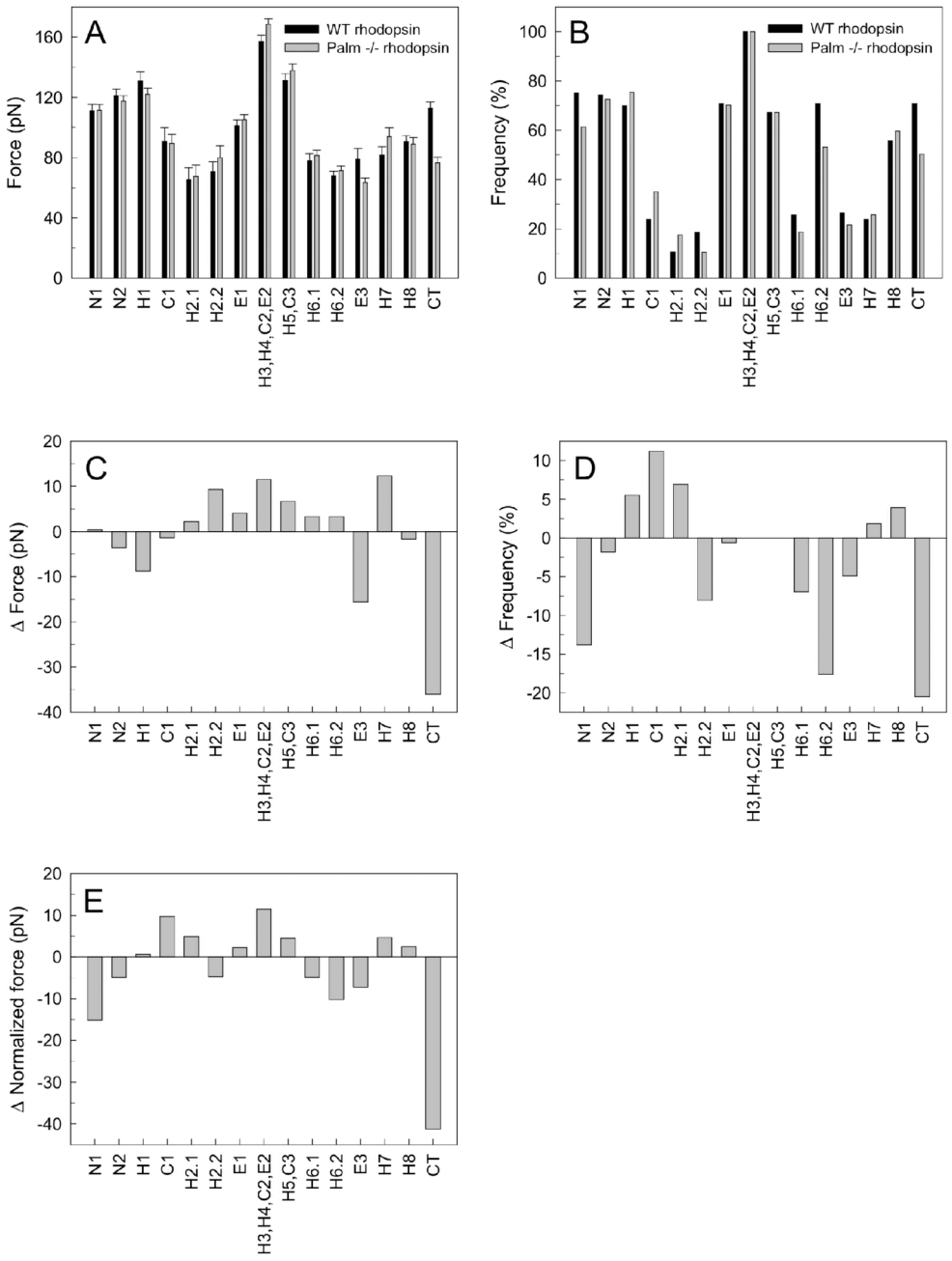

FIGURE 8.

Effect of palmitate groups on the molecular interactions of rhodopsin. Rod outer segment disc membranes were examined by single-molecule force spectroscopy to determine the effect of palmitate groups on the molecular interactions of rhodopsin. Force-distance traces were collected from samples prepared from mice expressing wild-type (WT) or palmitate-deficient (Palm −/−) rhodopsin. The number of force-distance traces analyzed for wild-type and palmitate-deficient rhodopsin was 113 and 171, respectively. Force peaks previously assigned in bovine rhodopsin were analyzed (15) (Figure 7A). (A) Average unfolding forces (± SEM) for each analyzed segment is shown for wild-type (black) and palmitate-deficient (gray) rhodopsin. (B) The frequency of detection of each analyzed segment is shown for wild-type

(black) and palmitate-deficient (gray) rhodopsin. (C, D, E) The difference in average unfolding force (C), detection frequency (D), and normalized force (E) between palmitate-deficient and wild-type rhodopsin is shown for each analyzed segment. In each case, a positive number denotes a larger value for palmitate-deficient rhodopsin. Normalized force was calculated by multiplying average unfolding force with detection frequency.

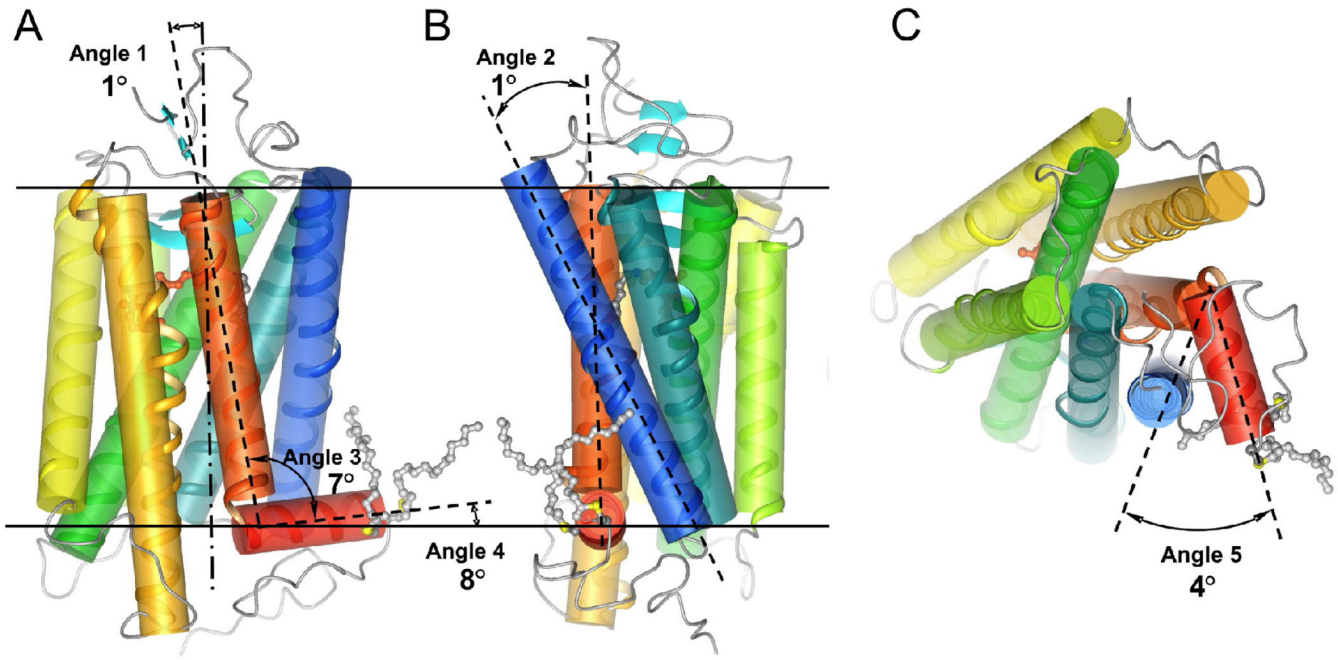

FIGURE 9.

Effect of palmitylation assessed by molecular dynamics simulations. Simulations were conducted to test the influence of palmitylation on the structure of rhodopsin. 32 independent simulations were conducted for 30 ns each: 16 simulations of rhodopsin with palmitylation and 16 simulations of rhodopsin without palmitylation. To determine the effect of palmitylation on the structure of rhodopsin surrounding the region of the palmitate groups, several angles were chosen and measured. Those angles (angles 1–5) are highlighted on the crystal structure of rhodopsin (Protein Data Bank ID: 1U19). Shown are two different side views of rhodopsin with horizontal lines denoting the border of the lipid bilayer (A and B) and a top view of rhodopsin from the cytoplasmic side (C). Helices are rainbow colored from blue (Helix 1) to orange-red (Helix 7), and red (Helix 8). The average value obtained in simulations for each angle and their standard deviations are as follows: angle 1 (Helix 7 to the normal of the membrane plane), 9.8°±2.8° (palmitylated) and 8.8°±2.7° (unpalmitylated); angle 2 (Helix 1 to Helix 7), 25.2°±3.4° (palmitylated) and 24.7°±2.6° (unpalmitylated); angle 3 (Helix 7 to Helix 8), 90.3°±5.9° (palmitylated) and 97.7°±7.9° (unpalmitylated), angle 4 (Helix 8 to the membrane plane), 8.2°±5.0° (palmitylated) and −0.2°±7.5° (unpalmitylated), and angle 5 (cytoplasmic end of Helix 1 to Helix 8), 51.5°±6.9° (palmitylated) and 55.5°±8.6° (unpalmitylated). The difference in the average value obtained for each angle between simulations of palmitylated and unpalmitylated rhodopsin is shown.